Journal of Physics: Conference Series **91** (2007) 012002 doi:10.1088/1742-6596/91/1/012002

An introduction to relativistic hydrodynamics

José A. Font

Departamento de Astronomía y Astrofísica, Universidad de Valencia, Dr. Moliner 50, 46100 Burjassot (Valencia), Spain

E-mail: j.antonio.font@uv.es

Abstract. We review formulations of the equations of (inviscid) general relativistic hydrodynamics and (ideal) magnetohydrodynamics, along with methods for their numerical solution. Both systems can be cast as first-order, hyperbolic systems of conservation laws, following the explicit choice of an Eulerian observer and suitable fluid and magnetic field variables. During the last fifteen years, the so-called (upwind) high-resolution shock-capturing schemes based on Riemann solvers have been successfully extended from classical to relativistic fluid dynamics, both special and general. Nowadays, general relativistic hydrodynamical simulations in relativistic astrophysics are routinely performed, particularly within the test-fluid approximation but also for dynamical spacetimes. While such advances also hold true in the case of the MHD equations, the astrophysical applications investigated so far are still limited, yet the field is bound to witness major developments in the near future. The article also presents a brief overview of numerical techniques, providing state-of-the-art examples of their applicability to general relativistic fluids and magneto-fluids in characteristic scenarios of relativistic astrophysics.

1. Introduction

Relativistic hydrodynamics is the part of physics devoted to the study of both, flows in which the velocities attained by individual particles or by the fluid as a whole approach the speed of light in vacuum, or those for which the strength of the gravitational field – either background or that generated by the matter itself, or both – is important enough to render mandatory a description in terms of Einstein's theory of gravity. These two extreme circumstances, far from being met by the flows present in our daily life, are routinely encountered in some violent places of our cosmos. In fact, almost any high-energy astrophysical phenomenon astronomers observe and investigate requires a relativistic treatment. Moreover, to understand their dynamics and evolution astrophysicists usually resort to mathematical and numerical models which incorporate relativistic hydrodynamics as a key building block. Scenarios involving compact objects such as supernova explosions leading to neutron stars, microquasars, active galactic nuclei, and coalescing neutron stars, all contain flows at (varying degrees of) relativistic speeds and, in many cases, strong shock waves. In particular, flow velocities as large as 99% of the speed of light are required to explain the apparent superluminal motion inferred in many of the observed jets in extragalactic radio sources associated with active galactic nuclei. A relativistic description of the matter hydrodynamics and of the gravity is also necessary in scenarios involving the gravitational collapse of massive stars to form black holes, or at the last stage of the coalescence of neutron

star binaries. Such events are believed to be the mechanisms responsible for long and short gamma-ray bursts, respectively, the most luminous events in the Universe after the Big Bang. Again, the flow speeds achieved in the highly collimated, jetted emission of a gamma-ray burst may amount to figures well beyond 99% times the speed of light. Last but not least, the presence of both relativistic flows and massive compact objects in the aforementioned astrophysical scenarios turns them into main sources of potentially detectable gravitational radiation. The direct detection of these elusive ripples in the curvature of spacetime, and the wealth of new information that could be extracted thereof, is one of the driving motivations of present-day research in relativistic astrophysics.

The investigation of the dynamics and evolution of such relativistic astrophysical systems strongly relies on the assistance of accurate, large-scale numerical simulations. This task is, however, daunting, as the governing equations to solve, the general relativistic hydrodynamics and magneto-hydrodynamics equations (GRHD/GRMHD hereafter) coupled to Einstein's equations, are rich in conceptual and technical difficulties. In some cases approximations are justifiable, as e.g. whenever the self-gravity of the fluid is negligible in comparison with the "background" gravitational field. Nowadays, such test-fluid approximation is highly developed numerically, particularly for the GRHD case. On the other hand, there has also been intense work in recent years on formulating and solving the MHD equations in general relativistic spacetimes (either background or dynamical), which has allowed for the first accurate simulations ever in the fields of gravitational collapse, black hole accretion and jet formation. Mathematically, as we shall see in this paper, the GRHD/GRMHD equations are nonlinear hyperbolic systems of balance laws. For such systems there exist solid mathematical foundations and highly sophisticated numerical methodology imported from computational fluid dynamics. A "preferred" choice among the various approaches at one's disposal are the so-called high-resolution shock-capturing schemes (HRSC hereafter), either upwind or central, and written in conservation form.

The aim of this paper is to present a brief overview of 3+1 formulations of general relativistic hydrodynamics and magneto-hydrodynamics, with an emphasis on their suitability for advanced numerical work with HRSC schemes. In this respect the paper is intended to provide the bare bones of such a broad topic, supplying pointers on further reading. The interested reader is addressed to more detailed review articles and monographs on the subject, such as those of [1, 2, 3, 4] regarding mathematical and numerical aspects of the GRHD/GRMHD equations, and [5, 6] regarding general issues on numerical methods for conservation laws. The paper is organized as follows: Section 2 discusses the equations of 3+1 general relativistic hydrodynamics. The corresponding GRMHD equations are considered in Section 3. Next, in Section 4 we give a short overview of the various formulations of Einstein's equations (within the 3+1 framework) that are most widely employed in current numerical simulations, incorporating explicitely in the equations the matter content. Section 5 discusses numerical methods for conservation laws, providing connections with the GRHD and GRMHD systems. Some astrophysical examples are mentioned in Section 6. Finally, the paper closes with a short summary in Section 7. Throughout the paper Greek indices are assumed to run from 0 to 3 while Latin indices run from 1 to 3; geometrized units $G = c = 1$ are used, and boldface letters indicate vectors.

2. General relativistic hydrodynamics equations

Undergraduate students in Physics are all familiar with the standard textbook derivation of the classical fluid (or gas) dynamics equations (see e.g. [7]) in which three basic physical principles are used, the conservation of mass, momentum (Newton's second law), and energy. To derive those equations two fundamental assumptions are made. First, fluid dynamics is supposed to deal with the behaviour of matter in the large (average quantities per unit volume), i.e. on a macroscopic scale large compared with the distance between fluid molecules. This permits not to take into account the molecular structure of fluids, a task reserved for the kinetic theory of gases. Even when an infinitesimal volume element is considered, it must be presumed that it is much smaller than the dimensions of the fluid, but still much larger than the distance between molecules. The second assumption presumes a perfectly continuous macroscopic behaviour of fluids, and physical quantities such as mass, density, or momentum contained within a given small volume are regarded as uniformly spread over that volume. Therefore, those quantities characterizing a fluid (in the continuum limit) are functions of time and space.

Under these two key assumptions the principles of conservation of mass, momentum, and energy within a given fluid volume element lead, respectively, to the equations of continuity, Euler's equation, and energy equation. These equations can be written in a compact way as a first-order, flux-conservative, hyperbolic system:

$$\frac{\partial \mathbf{U}}{\partial t} + \frac{\partial \mathbf{F}^i}{\partial x^i} = \mathbf{S}(\mathbf{U}), \tag{1}$$

where the state-vector $\mathbf{U}$, the vector of fluxes (along each direction i) $\mathbf{F}^i$, and the vector of (undifferentiated) source terms $\mathbf{S}$ read, respectively:

$$\mathbf{U} = (\rho, \rho v^j, e), \tag{2}$$

$$\mathbf{F}^i = (\rho v^i, \rho v^i v^i + p\delta^{ij}, (e+p)v^i), \tag{3}$$

$$\mathbf{S} = \left(0, -\rho\frac{\partial \Phi}{\partial x^j}, -\rho v^i \frac{\partial \Phi}{\partial x^i}\right). \tag{4}$$

In these equations ρ is the mass density, v^j is the velocity, e is the total (internal plus kinetic) energy, namely $e = \rho\varepsilon + \frac{1}{2}\rho\mathbf{v}^2$, ε being the specific internal energy, p is the (thermal) pressure, and δ^{ij} is Kronecker's delta. In addition, a conservative external force field (e.g. the gravitational field) is supposed to exist, $\mathbf{g} = -\nabla\Phi$, where Φ is the gravitational potential satisfying Poisson's equation, $\Delta\Phi = -4\pi G\rho$, where G is Newton's gravitational constant, and ∇ and Δ are the Nabla and Laplacian operators, respectively.

We note that in the above equations viscous effects have been explicitely neglected. Otherwise, Euler's equation would have to be replaced by Navier-Stokes' equation (no longer hyperbolic) and the energy equation would contain additional terms accounting for heat transfer and dissipation of kinetic energy. While their numerical description still represents a challenging task, viscous effects due to the transfer of momentum along velocity gradients by turbulence and thermal motions, should in general be considered in some representative astrophysical scenarios, namely accretion disks for which shearing motions or steep velocity gradients may appear. In addition, viscosity is also believed to play a significant role on the stability and dynamics of compact stars, destroying differential rotation in rapidly rotating neutron stars or suppressing the bar-mode instability as well as gravitational-radiation driven instabilities.

The distinctive property of hyperbolic, partial differential equations is to have finite propagation speed: of information. This can travel with a maximum speed given by the largest of the characteristic curves of the system. The range of influence of the solution is hence bounded by the eigenvalues of the Jacobian matrix of the system, $\lambda_\pm = v^i \pm c_s$, where c_s is the sound speed. This property has consequences on the design of numerical procedures to solve hyperbolic equations (see Section 5 below).

The corresponding GRHD equations which would replace the above classical hydrodynamics equations in situations involving strong gravitational fields or flows approaching the speed of light are also described by local conservation laws, of momentum and energy on the one hand, encoded in the stress-energy tensor $T^{\mu\nu}$, and of the matter current density on the other, J^μ (the continuity equation):

$$\nabla_\mu T^{\mu\nu} = 0, \qquad \nabla_\mu J^\mu = 0. \tag{5}$$

Here, ∇_μ stands for the 4-dimensional covariant derivative. The current density is given by $J^\mu = \rho u^\mu$, where u^μ is the 4-velocity of the fluid and ρ its rest-mass density. As customary we assume hereafter a perfect fluid stress-energy tensor

$$T^{\mu\nu} = \rho h u^\mu u^\nu + p g^{\mu\nu}, \tag{6}$$

where h stands for the specific enthalpy, $h = 1 + \varepsilon + p/\rho$, and $g_{\mu\nu}$ is the spacetime metric tensor.

The previous system of equations, either classical or relativist, is closed once an equation of state (EOS hereafter) is chosen, namely a thermodynamical relation connecting the pressure to two independent state variables, e.g., $p = p(\rho, \varepsilon)$. The available EOSs have become sophisticated enough to take into account physical and chemical processes such as molecular interactions, quantization, relativistic effects, nuclear physics, etc. Nevertheless, the most widely employed EOSs in numerical simulations in astrophysics are the *ideal fluid* EOS, $p = (\Gamma - 1)\rho\varepsilon$, where Γ is the adiabatic index, and the *polytropic* EOS (e.g. to build equilibrium stellar models), $p = K\rho^\Gamma \equiv K\rho^{1+1/N}$, K being the polytropic constant and N the polytropic index. State-of-the-art, microphysical EOSs that describe the interior of compact stars at nuclear matter densities have also been developed. While they are being increasingly used in the numerical modelling of relativistic stars, the true EOS of neutron star interiors remains still largely unknown, as reproducing the associated densities and temperatures is not amenable to laboratory experimentation. In the test-fluid approximation where the fluid's self-gravity is ignored, the dynamics of the matter fields is completely described by the previous conservation laws and the EOS. Whenever such approximation does not hold, these equations must be solved in conjunction with Einstein's equations for the gravitational field which describe the evolution of a dynamical spacetime.

Most approaches for the numerical solution of the general relativistic hydrodynamics equations adopt spacelike foliations of the spacetime, within the so-called 3+1 (Cauchy) formulation [8, 9]. However, covariant forms of these equations are also available in ways well suited for advanced numerical methods [10, 11]. The interested reader is addressed to [4] for a review of the latter formulations, which will not be covered here. Introducing a coordinate chart (x^0, x^i) the 3+1 line element (see e.g. [12] for details) reads

$$ds^2 = -(\alpha^2 - \beta_i\beta^i)dx^0dx^0 + 2\beta_i dx^i dx^0 + \gamma_{ij}dx^i dx^j, \tag{7}$$

where α is the lapse function, β^i is the shift vector, and γ_{ij} is the spatial 3-metric induced on each spacelike slice. Therefore, the above (covariant) conservation equations 5 read

$$\frac{\partial}{\partial x^\mu}\sqrt{-g}J^\mu \ = 0, \tag{8}$$

$$\frac{\partial}{\partial x^\mu}\sqrt{-g}T^{\mu\nu} = \ -\sqrt{-g}\Gamma^\nu_{\mu\lambda}T^{\mu\lambda}\,, \tag{9}$$

where $g = \det(g_{\mu\nu}) = \alpha\sqrt{\gamma}$, $\gamma = \det(\gamma_{ij})$, and $\Gamma^\nu_{\mu\lambda}$ are the so-called Christoffel symbols.

The traditional approach for relativistic hydrodynamics on spacelike hypersurfaces is based on Wilson's pioneering work [8]. In this formalism the equations were written as a set of advection equations, sidestepping an important guideline for the formulation of nonlinear hyperbolic systems of equations, namely the preservation of their conservation form. This feature is necessary to guarantee correct evolution in regions of sharp entropy generation, i.e. shocks, a common feature of nonlinear hyperbolic equations. (However, in the absence of such features, non-conservative formulations are equivalent to conservative ones.) The approach is simple to implement and has been widely used over the years in numerical relativistic astrophysics.

On the other hand, a numerical scheme in conservation form allows naturally for shock-capturing. Writing the relativistic hydrodynamic equations as a system of conservation laws, identifying the suitable vector of unknowns, and building up an approximate Riemann solver, permitted the extension of modern HRSC schemes from classical fluid dynamics into the realm of relativity [13] (see also [10]). The main theoretical ingredients to construct such a HRSC scheme in 3+1 general relativity can be found in [9]. In this reference the GRHD equations were written as a first-order, flux-conservative, hyperbolic system, amenable to numerical work [4]:

$$\frac{1}{\sqrt{-g}}\left(\frac{\partial\sqrt{\gamma}\mathbf{U}(\mathbf{w})}{\partial x^0}+\frac{\partial\sqrt{-g}\mathbf{F}^i(\mathbf{w})}{\partial x^i}\right)=\mathbf{S}(\mathbf{w}), \tag{10}$$

reminiscent of Eq. (1) save for the presence of geometrical terms in $\sqrt{\gamma}$ and $\sqrt{-g}$. With respect to the Eulerian observer and in terms of the *primitive variables*, $\mathbf{w} = (\rho, v^i, \varepsilon)$, the state vector $\mathbf{U}$ (conserved variables) and the vectors of fluxes $\mathbf{F}$ and source terms $\mathbf{S}$, are given by

$$\mathbf{U}(\mathbf{w}) \ = (D, S_j, \tau), \tag{11}$$

$$\mathbf{F}^i(\mathbf{w}) = \left(D\tilde{v}^i, S_j\tilde{v}^i + p\delta^i_j, \tau\tilde{v}^i + pv^i\right), \tag{12}$$

$$\mathbf{S}(\mathbf{w}) \ = \left(0, T^{\mu\nu}\left(\frac{\partial g_{\nu j}}{\partial x^\mu} - \Gamma^\delta_{\nu\mu}g_{\delta j}\right), \alpha\left(T^{\mu 0}\frac{\partial \ln\alpha}{\partial x^\mu} - T^{\mu\nu}\Gamma^0_{\nu\mu}\right)\right), \tag{13}$$

where $\tilde{v}^i = v^i - \beta^i/\alpha$. The conserved quantities in Eq. (11) are the relativistic densities of mass, momenta, and energy, respectively, defined as $D = \rho W$, $S_j = \rho h W^2 v_j$, and $\tau = \rho h W^2 - p - D$. In these expressions W stands for the Lorentz factor, defined as $W = \alpha u^0$. We note that in the energy equation the continuity equation has been subtracted in order to properly recover the Newtonian limit.

It is worth noting that the presence of the Lorentz factor in the convective terms of the hydrodynamics equations (and of the pressure in the specific enthalpy) makes the relativistic equations much more coupled than their Newtonian counterparts. This has significant implications in their numerical solution, particularly if nonconservative approaches are used. The most important consequence is the unavoidable numerical

limitations when dealing with situations involving ultrarelativistic flows. While implicit schemes were proposed to capture more accurately such coupling [14], restrictions persisted for values of $W \sim 10$ and larger. Ultrarelativistic flows could only be handled (with explicit schemes) once conservative formulations were adopted [13, 10, 9].

HRSC numerical schemes based on Riemann solvers (see below and [5, 6]) use the local characteristic structure of the hyperbolic system of equations. For the previous system, Eq. (10), this information was provided in [9] (see also [15, 4]). The eigenvalues (characteristic speeds) are all real but not distinct, one of them showing a threefold degeneracy, and complete sets of right- and left-eigenvectors exist. The above system satisfies, thus, the definition of hiperbolicity (yet it is not either strictly hyperbolic nor symmetric hyperbolic in its particular form). We note, however, an important difference with the Newtonian case, namely the existence of couplings in the eigenvalues along a given direction, say the $x-$direction, with components of the velocity field transversal to v^x:

$$\lambda_\pm = \frac{\alpha}{1-v^2 c_s^2}\left\{ v^x(1-c_s^2) \right. \\ \left. \pm \; c_s\sqrt{(1-v^2)[\gamma^{xx}(1-v^2c_s^2)-v^x v^x(1-c_s^2)]}\right\} - \beta^x \,. \qquad (14)$$

In this expression such coupling is apparent through the modulus of the velocity, $v^2 = \gamma_{ij}v^i v^j$. In addition, even in the purely one-dimensional case, $\mathbf{v} = (v^x, 0, 0)$, the flow speed and the sound speed are connected through the relativistic addition of velocities $\lambda_\pm = \frac{v^x \pm c_s}{1 \pm v^x c_s}$, instead of the Galilean addition present in the Newtonian case, $\lambda_\pm = v^x \pm c_s$. Finally, we note that degeneracies in the entire set of GRHD eigenvalues occur as the flow speed reaches the speed of light and when the lapse function goes to zero (which is purely a gauge effect), e.g. at the horizon of a black hole (which behaves as a sonic sphere).

3. General relativistic magneto-hydrodynamics equations

General relativistic MHD is concerned with the dynamics of relativistic, electrically conducting fluids (plasma) in the presence of magnetic fields. Here, we discuss only purely *ideal* GRMHD, neglecting effects due to viscosity and heat conduction in the limit of infinite conductivity (the fluid is assumed to be a perfect conductor with no resistivity). We note that there are examples in astrophysics in which resistivity effects may become important and ideal MHD may not be valid to describe the dynamics of the plasma, typically in situations involving dilute accretion flows. For example, the Hall effect in protostellar disks is one of those effects, with significant implications regarding the so-called magneto-rotational instability, the mechanism believed to regulate angular momentum transport in disks through sustained accretion. In addition, reconnection of magnetic field lines (in e.g. solar flares) is another important non-ideal MHD effect which may appear in turbulent plasmas near the scale of energy dissipation. When the fluid is no longer a perfect conductor kinetic effects become important and the so-called particle-in-cell methods (not discussed here) are usually employed instead of finite volume methods.

As the GRHD equations discussed in the preceding section, the GRMHD equations can also be cast in first-order, flux-conservative, hyperbolic form. In recent years there has been intense work on formulating and solving numerically the MHD equations in general relativistic spacetimes, either background or dynamical [16, 17,

18, 19, 20, 21, 22, 23, 24, 25]. Both, artificial viscosity and HRSC schemes have been developed and most of the astrophysical applications previously attempted with no magnetic fields included are currently being revisited, namely for studies of gravitational collapse, neutron star dynamics, black hole accretion, and jet formation. The discussion reported in this section follows the particular derivation of these equations as presented in [23] to which the reader is addressed for further details.

In terms of the (Faraday) electromagnetic tensor $F^{\mu\nu}$, defined as

$$F^{\mu\nu} = U^\mu E^\nu - U^\nu E^\mu - \eta^{\mu\nu\lambda\delta} U_\lambda B_\delta \,, \tag{15}$$

Maxwell's equations read

$$\nabla_\nu {}^*F^{\mu\nu} = 0, \qquad \nabla_\nu F^{\mu\nu} = \mathcal{J}^\mu, \tag{16}$$

where the dual of the Faraday tensor is ${}^*F^{\mu\nu} = \frac{1}{2}\eta^{\mu\nu\lambda\delta}F_{\lambda\delta}$, and $\eta^{\mu\nu\lambda\delta} = \frac{1}{\sqrt{-g}}[\mu\nu\lambda\delta]$, with $[\mu\nu\lambda\delta]$ being the completely antisymmetric Levi-Civita symbol. Quantities E^μ and B^μ appearing in the Faraday tensor stand for the electric and magnetic fields measured by a generic observer with 4-velocity U^μ, respectively. Furthermore, $\mathcal{J}^\mu$ is the electric 4-current, defined as $\mathcal{J}^\mu = \rho_q u^\mu + \sigma F^{\mu\nu}u_\nu$, where ρ_q is the proper charge density and σ is the electric conductivity.

Maxwell's equations can be simplified if the fluid is a perfect conductor. In this case σ is infinite and, to keep the current finite, the term $F^{\mu\nu}u_\nu$ in the definition of the 4-current must vanish, which results in $E^\mu = 0$ for a comoving observer. This case corresponds to the so-called ideal MHD condition. Under this assumption the electric field measured by the Eulerian observer has components

$$E^0 = 0, \qquad E^i = -\alpha\eta^{0ijk}v_j B_k, \tag{17}$$

and Maxwell's equations $\nabla_\nu {}^*F^{\mu\nu} = 0$ reduce to the divergence-free condition of the magnetic field plus the induction equation for the evolution of the magnetic field

$$\frac{\partial(\sqrt{\gamma}B^i)}{\partial x^i} = 0, \tag{18}$$

$$\frac{1}{\sqrt{\gamma}}\frac{\partial}{\partial x^0}(\sqrt{\gamma}B^i) = \frac{1}{\sqrt{\gamma}}\frac{\partial}{\partial x^j}\{\sqrt{\gamma}[\alpha\tilde{v}^i B^j - \alpha\tilde{v}^j B^i]\}. \tag{19}$$

In addition, for a fluid endowed with a magnetic field, the stress-energy tensor can be naturally split in two parts, one corresponding to the fluid and a second piece corresponding to the electromagnetic field, $T^{\mu\nu} = T^{\mu\nu}_{\rm Fluid} + T^{\mu\nu}_{\rm EM}$, where $T^{\mu\nu}_{\rm Fluid}$ is given by Eq. (6) for a perfect fluid. On the other hand $T^{\mu\nu}_{\rm EM}$ can be built from the Faraday tensor as follows:

$$T^{\mu\nu}_{\rm EM} = F^{\mu\lambda}F^\nu_\lambda - \frac{1}{4}g^{\mu\nu}F^{\lambda\delta}F_{\lambda\delta}, \tag{20}$$

which, in ideal MHD, can be rewritten as

$$T^{\mu\nu}_{\rm EM} = \left(u^\mu u^\nu + \frac{1}{2}g^{\mu\nu}\right)b^2 - b^\mu b^\nu, \tag{21}$$

where b^μ is the magnetic field measured by the observer comoving with the fluid and $b^2 = b^\nu b_\nu$. The total stress-energy tensor is thus given by

$$T^{\mu\nu} = \rho h^* u^\mu u^\nu + p^* g^{\mu\nu} - b^\mu b^\nu, \tag{22}$$

where we have introduced the following definitions, $p^* = p + b^2/2$ and $h^* = h + b^2/\rho$.

Following [23] the conservation equations for the energy-momentum tensor, together with the continuity equation and the equation for the evolution of the

magnetic field, can be written as a first-order, flux-conservative, hyperbolic system equivalent to (10). The state vector and the vector of fluxes of the GRMHD system of equations read:

$$\mathbf{U}(\mathbf{w}) = (D, S_j, \tau, B^k), \tag{23}$$

$$\mathbf{F}^i(\mathbf{w}) = (D\tilde{v}^i, S_j\tilde{v}^i + p^*\delta^i_j - b_j B^i/W, \tau\tilde{v}^i + p^* v^i - \alpha b^0 B^i/W, \tilde{v}^i B^k - \tilde{v}^k B^i), \tag{24}$$

where the conserved quantities are now defined as $D = \rho W$, $S_j = \rho h^* W^2 v_j - \alpha b^0 b_j$, and $\tau = \rho h^* W^2 - p^* - \alpha^2 (b^0)^2 - D$. The corresponding vector of sources coincides with the one given by Eq. (13) save for the use of the complete (fluid plus electromagnetic field) stress-energy tensor (the magnetic field evolution equation is source-free). We note that expressions (23) and (24) contain components of the magnetic field measured by both, a comoving observer and an Eulerian observer. The two are related by

$$b^0 = \frac{W B^i v_i}{\alpha}, \qquad\qquad b^i = \frac{B^i + \alpha b^0 u^i}{W}. \tag{25}$$

The wave structure of the above GRMHD hyperbolic system is, understandably, more involved than that corresponding to the GRHD case. Anile and Pennisi [26] and Anile [1] (see also [27]) have studied the characteristic structure of these equations (eigenvalues, right- and left-eigenvectors) in the (10-dimensional) space of covariant variables (u_μ, b_μ, p, s), where s is the entropy. It was found that only the entropic waves and the Alfvén waves are explicit, namely (for the formulation of [23] discussed in this section)

$$\lambda^i_e = \alpha v^i - \beta^i\,, \tag{26}$$

$$\lambda^i_{a\pm} = \frac{b^i \pm \sqrt{\rho h + B^2}\, u^i}{b^0 \pm \sqrt{\rho h + B^2}\, u^0}\,, \tag{27}$$

while the (fast and slow) magnetosonic waves are given by the numerical solution (through a root-finding procedure) of a quartic characteristic equation. We note that as a result of working with the unconstrained, 10×10 system of equations, there appear superfluous eigenvalues associated with unphysical waves which need to be removed (the entropy waves as well as the Alfvén waves appear as double roots). Any attempt to develop a numerical procedure based on the wave structure of the RMHD equations must hence remove these nonphysical waves (and the corresponding eigenvectors) from the wave decomposition. In the particular case of special relativistic MHD, [28] and [29] eliminate the unphysical eigenvectors by enforcing the waves to preserve the values of the invariants $u^\mu u_\mu = -1$ and $u^\mu b_\mu = 0$, as suggested by [1]. Correspondingly, [30] selects the physical eigenvectors by comparing with the equivalent expressions in the nonrelativistic limit.

Among the magnetosonic waves, the two solutions with maximum and minimum speeds are called *fast* magnetosonic waves $\lambda^i_{f\pm}$, and the two solutions in between are the so-called *slow* magnetosonic waves $\lambda^i_{s\pm}$. The seven waves can be ordered as follows

$$\lambda^i_{f-} \le \lambda^i_{a-} \le \lambda^i_{s-} \le \lambda^i_e \le \lambda^i_{s+} \le \lambda^i_{a+} \le \lambda^i_{f+}, \tag{28}$$

which defines the domain of dependence of the GRMHD system.

To close this section we note that, as in the classical case, the relativistic MHD equations have degenerate states in which two or more wavespeeds coincide, which breaks the strict hyperbolicity of the system and may affect numerical schemes for its solution. These degeneracies have been analyzed by [28], who found that, with respect

to the fluid rest frame, the degeneracies in both classical and relativistic MHD are the same: either the slow and Alfvén waves have the same speed as the entropy wave when propagating perpendicularly to the magnetic field (Degeneracy I), or the slow or the fast wave (or both) have the same speed as the Alfvén wave when propagating in a direction aligned with the magnetic field (Degeneracy II). On the other hand, [31] has derived a covariant characterization of such degenerate states which can be checked in any reference frame. In addition, [31] has also worked out a single set of right and left eigenvectors which are regular and span a complete basis in any physical state, including degenerate states. Such renormalization procedure can be seen as a relativistic generalization of the work performed by [32] in classical MHD.

4. Formulations of Einstein's equations for nonvacuum spacetimes

Simulations of astrophysical systems in the strong gravity regime have recently benefited from advances in the formulations of both the GRHD and GRMHD equations, but also from important breakthroughs in the arena of the gravitational field equations themselves, both at the theoretical and at the numerical fronts. Indeed, formulations of Einstein's equations suitable for long-term stable numerical simulations are available and have proved adequate in a variety of scenarios, including remarkably merging binary black holes, the archetypal and most challenging problem in Numerical Relativity (see [33] and references therein). In the following we briefly review some of the formulations which are most commonly used nowadays.

4.1. CFC metric equations

Until recently the workhorse formulation of Einstein's equations in Numerical Relativity has been the so-called ADM 3+1 formulation (see e.g. [34] and references therein). Given a choice of lapse function α and shift vector β^i, Einstein's equations in the 3+1 formalism split into evolution equations for the 3-metric γ_{ij} and constraint equations that must be satisfied on any time slice. The evolution equations read

$$\partial_t \gamma_{ij} = -2\alpha K_{ij} + \nabla_i \beta_j + \nabla_j \beta_i \,, \tag{29}$$

$$\partial_t K_{ij} = -\nabla_i \nabla_j \alpha + \alpha \left(R_{ij} + K\ K_{ij} - 2K_{im} K^m_j \right) + \beta^m \nabla_m K_{ij} + K_{im} \nabla_j \beta^m + K_{mj} \nabla_i \beta^m - 4\pi\alpha \left(2S_{ij} - \gamma_{ij} S + \rho_{\rm E} \gamma_{ij} \right) , \tag{30}$$

where K_{ij} is the extrinsic curvature of the 3–dimensional time slice, R_{ij} is the Ricci tensor of the induced 3–metric, and ∇_i is the covariant derivative associated with γ_{ij}. In addition, the Hamiltonian and momentum constraint equations read, respectively

$$R + K^2 - K^{ij} K_{ij} = 16\pi \rho_{\rm E} \,, \tag{31}$$

$$\nabla_i \left(K^{ij} - \gamma^{ij} K \right) = 8\pi S^j , \tag{32}$$

where R is the Ricci scalar, and K is the trace of the extrinsic curvature.

From the energy-momentum tensor $T^{\mu\nu}$ it is possible to build the matter quantities appearing in the above expressions: the total energy $\rho_{\rm E} \equiv n^\mu n^\nu T_{\mu\nu} = \alpha^2 T^{00}$, the momenta $S_i \equiv -\perp^\mu_i n^\nu T_{\mu\nu} = -\frac{1}{\alpha}(T_{0i} - T_{ij}\beta^j)$, and the spatial components of the energy-momentum tensor $S_{ij} \equiv \perp^\mu_i \perp^\nu_j T_{\mu\nu}$ (with S denoting its trace, $S = S^i_i$). To this aim we must use the projection operator $\perp^\mu_\nu = g^\mu_\nu + n^\mu n_\nu$ and the unit four-vector n^μ normal to the hypersurface.

If the spatial 3-metric is assumed to be conformally flat, i.e. $\gamma_{ij} = \phi^4 \delta_{ij}$, with ϕ being the conformal factor, and under the additional assumption of a maximally-sliced spacetime ($K = 0$), the ADM 3+1 equations reduce to a system of five coupled, nonlinear elliptic equations for the lapse function, the conformal factor, and the shift vector [35, 36]:

$$\hat{\Delta}\phi = -2\pi\phi^5 \left(\rho h W^2 - p + \frac{K_{ij}K^{ij}}{16\pi} \right), \tag{33}$$

$$\hat{\Delta}(\alpha\phi) = 2\pi\alpha\phi^5 \left(\rho h(3W^2 - 2) + 5p + \frac{7K_{ij}K^{ij}}{16\pi} \right), \tag{34}$$

$$\hat{\Delta}\beta^i = 16\pi\alpha\phi^4 S^i + 2\phi^{10} K^{ij} \hat{\nabla}_j \left(\frac{\alpha}{\phi^6} \right) - \frac{1}{3} \hat{\nabla}^i \hat{\nabla}_k \beta^k, \tag{35}$$

where $\hat{\nabla}_i$ and $\hat{\Delta}$ are the flat space Nabla and Laplace operators, respectively. (The hat symbol is used to denote flat spacetime operators.)

The simplified Einstein's equations introduced by the conformally-flat condition (CFC hereafter) are adequate in situations for which deviations from spherical symmetry are not significant. The satisfactory accuracy of the CFC approximation has been tested in various works, namely for stellar core collapse and equilibrium models of neutron stars [37, 38, 39, 40, 41, 42], as well as for binary neutron star mergers [43, 44]. It has been shown that the spacetime of rapidly (uniformly or differentially) rotating neutron star models is very well approximated by the CFC metric. Its accuracy degrades only in extreme cases, such as rapidly rotating massive neutron stars or black holes.

4.2. CFC+ metric equations

The above CFC system of equations has been recently extended by [45] through the incorporation of additional degrees of freedom in the approximation, which render the spacetime metric exact up to the second post-Newtonian order. Despite the original CFC system of metric equations (33)-(35) is augmented with additional equations, the final system in this new CFC+ formulation is still elliptic.

The natural way of improving the CFC approximation is through a post-Newtonian expansion of the traceless part of the 3-metric:

$$\gamma_{ij} = \phi^4 \hat{\gamma}_{ij} + h_{ij}^{\rm TT} = \gamma_{ij}^{\rm CFC} + \left[h_{ij}^{\rm 2PN} + \mathcal{O}\left(\frac{1}{c^4} \right) \right], \tag{36}$$

where $h_{ij}^{\rm 2PN}$ is the leading order in the expansion of $h_{ij}^{\rm TT}$. The CFC+ metric is obtained by truncating Eq. (36) at second post-Newtonian order in the traceless and transverse part. We note that CFC+ becomes exact for spherically symmetric spacetimes, just as CFC does, since in this case the TT part vanishes, while in a general nonspherical spacetime, CFC+ behaves as a second post-Newtonian approximation of the metric.

The computation of $h_{ij}^{\rm 2PN}$ can be simplified by introducing auxiliary potentials that are solutions of scalar/vector/tensor Poisson equations [45]. The (lengthy) derivation of the CFC+ equations is described in detail in [45]. Here, we simply summarize the main steps in the procedure to calculate the final CFC+ metric:

(i) Calculate "Newtonian" potential (one Poisson equation):

$$\hat{\Delta} U = -4\pi G D^{\dagger}, \tag{37}$$

where the dagger symbol indicates "densitized" quantities, i.e. $D^\dagger = \sqrt{\bar{\gamma}}D$, where $\bar{\gamma} = \gamma/\hat{\gamma}$, $\hat{\gamma}$ being the determinant of the flat 3-metric.

(ii) Calculate intermediate (scalar, vector, and tensor) potentials (16 linear Poisson equations):

$$\hat{\Delta}\mathcal{S} = -4\pi\frac{S_i^\dagger S_j^\dagger}{D^\dagger}x^i x^j, \tag{38}$$

$$\hat{\Delta}\mathcal{S}_i = \left[-4\pi\frac{S_i^\dagger S_j^\dagger}{D^\dagger} - \hat{\nabla}_i U\hat{\nabla}_j U\right]x^j, \tag{39}$$

$$\hat{\Delta}\mathcal{T}_i = \left[-4\pi\frac{S_j^\dagger S_k^\dagger}{D^\dagger} - \hat{\nabla}_j U\hat{\nabla}_k U\right]\hat{\gamma}^{jk}\hat{\gamma}_{il}x^l, \tag{40}$$

$$\hat{\Delta}\mathcal{R}_i = \hat{\nabla}_i(\hat{\nabla}_j U\hat{\nabla}_k U x^j x^k), \tag{41}$$

$$\hat{\Delta}\mathcal{S}_{ij} = -4\pi\frac{S_i^\dagger S_j^\dagger}{D^\dagger} - \hat{\nabla}_i U\hat{\nabla}_j U, \tag{42}$$

where x^i denote the coordinates and where, as in Eq. (37), the superscript † in the hydrodynamical fields is used to indicate 'densitized' fields, i.e. multiplied by $\sqrt{\bar{\gamma}}$.

(iii) Calculate $h_{ij}^{\rm TT}$:

$$\begin{aligned} h_{ij}^{\rm TT} &= \frac{1}{2}\mathcal{S}_{ij} - 3x^k\hat{\nabla}_{(i}\mathcal{S}_{j)k} + \frac{5}{4}\hat{\gamma}_{jm}x^m\hat{\nabla}_i\left(\hat{\gamma}^{kl}\mathcal{S}_{kl}\right) + \frac{1}{4}x^k x^l\hat{\nabla}_i\hat{\nabla}_j\mathcal{S}_{kl} \\ &+ 3\hat{\nabla}_{(i}\mathcal{S}_{j)} - \frac{1}{2}x^k\hat{\nabla}_i\hat{\nabla}_j\mathcal{S}_k + \frac{1}{4}\hat{\nabla}_i\hat{\nabla}_j\mathcal{S} - \frac{5}{4}\hat{\nabla}_i\mathcal{T}_j - \frac{1}{4}\hat{\nabla}_i\mathcal{R}_j \\ &+ \hat{\gamma}_{ij}\left[\frac{1}{4}\hat{\gamma}^{kl}\mathcal{S}_{kl} + x^k\hat{\gamma}^{lm}\hat{\nabla}_m\mathcal{S}_{kl} - \hat{\gamma}^{kl}\hat{\nabla}_k\mathcal{S}_l\right], \end{aligned} \tag{43}$$

where subindex (ij) indicates symmetrization with respect to the two indices.

(iv) Calculate the modified CFC equations (5 nonlinear Poisson-like equations):

$$\begin{aligned} \hat{\Delta}(\alpha\phi) &= 2\pi\alpha\phi^5\left(\rho h(3W^2-2) + 5p + \frac{7K_{ij}K^{ij}}{16\pi}\right) \\ &- \frac{1}{c^2}\hat{\gamma}^{ik}\hat{\gamma}^{jl}\,h_{ij}^{\rm TT}\hat{\nabla}_k\hat{\nabla}_l U, \end{aligned} \tag{44}$$

$$\hat{\Delta}\phi = -2\pi\phi^5\left(\rho h W^2 - p + \frac{K_{ij}K^{ij}}{16\pi}\right), \tag{45}$$

$$\hat{\Delta}\beta^i = 16\pi\alpha\phi^4 S^i + 2\hat{K}^{ij}\hat{\nabla}_j\left(\frac{\alpha}{\phi^6}\right) - \frac{1}{3}\hat{\nabla}^i\hat{\nabla}_k\beta^k,$$

with

$$\hat{K}_{ij} = \frac{1}{2\alpha}\left(\hat{\nabla}_i\beta_j + \hat{\nabla}_j\beta_i - \frac{2}{3}\gamma_{ij}\hat{\nabla}_k\beta^k\right) \equiv \phi^{10}K_{ij}\,, \tag{46}$$

$$K_{ij}K^{ij} = \frac{1}{\phi^{12}}\hat{K}_{ij}\hat{K}^{ij}. \tag{47}$$

(v) Finally, calculate the metric components:

$$g_{ij} = \gamma_{ij} = \phi^4\hat{\gamma^{ij}} + h_{ij}^{\rm TT}, \tag{48}$$

$$g_{00} = \gamma_{ij}\beta^j\beta^i - \alpha^2, \tag{49}$$

$$g_{0i} = \beta_i. \tag{50}$$

We note that the main limitation of both CFC and CFC+ is the fact that the gravitational wave degrees of freedom are lost in the approximations made. As a result, gravitational waves have to be extracted in an approximate way *a posteriori* directly from the sources (e.g. resorting to the standard quadrupole formula). CFC+ has been applied to axisymmetric simulations of pulsations in rotating neutron stars and rotational stellar core collapse to a proto-neutron star, where it was found that all matter and metric quantities show only minute differences with respect to CFC [45]. Needless to say, in scenarios where the CFC approximation is expected to become increasingly inaccurate, CFC+ would yield results which are closer to full general relativity.

4.3. BSSN metric equations

The ADM 3+1 metric equations have been shown over the years to be intrinsically unstable for long-term numerical simulations, especially for those dealing with black hole spacetimes. In the last 15 years there have been diverse attempts to reformulate those equations into forms better suited for numerical investigations (see [46, 47, 34] and references therein). Among the various approaches proposed, the so-called BSSN reformulation of the ADM system [46, 47] stands as very appropriate for long-term stable numerical work.

The main idea behind this approach is to remove the mixed second order derivatives appearing in the definition of the Ricci tensor by introducing auxiliary variables so that the evolution equations look like wave equations for the 3-metric and the extrinsic curvature. To achieve this the BSSN formulation makes use of a conformal decomposition of the 3-metric, $\tilde{\gamma}_{ij} = e^{-4\phi}\gamma_{ij}$ and of the trace-free part of the extrinsic curvature, $A_{ij} = K_{ij} - \gamma_{ij}K/3$, with the conformal factor ϕ chosen to satisfy $e^{4\phi} = \gamma^{1/3} \equiv \det(\gamma_{ij})^{1/3}$. In this formulation, as shown in [47], in addition to the evolution equations for the conformal 3-metric $\tilde{\gamma}_{ij}$ and the conformal-traceless extrinsic curvature variables $\tilde{A}_{ij} = e^{-4\phi}(K_{ij} - \gamma_{ij}K/3)$, there are evolution equations for the conformal factor ϕ, the trace of the extrinsic curvature K, and the "conformal connection functions" $\tilde{\Gamma}^i$ [47], defined as

$$\tilde{\Gamma}^a = \tilde{\gamma}^{ij}\tilde{\Gamma}^a_{ij} = -\partial_i\tilde{\gamma}^{ai}. \tag{51}$$

The final set of BSSN evolution equations reads:

$$(\partial_t - \mathcal{L}_\beta)\tilde{\gamma}_{ij} = -2\alpha\tilde{A}_{ij}, \tag{52}$$

$$(\partial_t - \mathcal{L}_\beta)\phi = -\frac{1}{6}\alpha K, \tag{53}$$

$$(\partial_t - \mathcal{L}_\beta)K = -\gamma^{ij}\nabla_i\nabla_j\alpha + \alpha\left[\tilde{A}_{ij}\tilde{A}^{ij} + \frac{1}{3}K^2 + \frac{1}{2}\left(\rho_{\rm E} + S\right)\right], \tag{54}$$

$$\begin{aligned}(\partial_t - \mathcal{L}_\beta)\tilde{A}_{ij} = {} & e^{-4\phi}\left[-\nabla_i\nabla_j\alpha + \alpha\left(R_{ij} - S_{ij}\right)\right]^{\rm TF} \\ & + \alpha\left(K\tilde{A}_{ij} - 2\tilde{A}_{il}\tilde{A}^l_j\right),\end{aligned} \tag{55}$$

$$\begin{aligned}(\partial_t - \mathcal{L}_\beta)\tilde{\Gamma}^i = {} & -2\tilde{A}^{ij}\partial_j\alpha \\ & + 2\alpha\left(\tilde{\Gamma}^i_{jk}\tilde{A}^{kj} - \frac{2}{3}\tilde{\gamma}^{ij}\partial_j K - \tilde{\gamma}^{ij}S_j + 6\tilde{A}^{ij}\partial_j\phi\right) \\ & + \partial_j\left(\beta^l\tilde{\partial}_l\tilde{\gamma}^{ij} - 2\tilde{\gamma}^{m(j}\partial_m\beta^{i)} + \frac{2}{3}\tilde{\gamma}^{ij}\partial_l\beta^l\right),\end{aligned} \tag{56}$$

where $\mathcal{L}_\beta$ stands for the Lie derivative.

BSSN (or slight modifications thereof) is currently the standard 3+1 formulation in Numerical Relativity [34]. Long-term stable applications include strongly gravitating systems such as neutron stars (both, isolated [48, 49] and binaries [50]) and single and *binary black holes*. Such binary black hole evolutions, possibly the grandest challenge of Numerical Relativity since the very beginning of the field, have only been possible very recently (see [33] and references therein).

5. Numerical methods for conservation laws

As we have discussed in Sections 2 and 3, the GRHD/GRMHD equations constitute nonlinear hyperbolic systems of conservation laws, just as their classical (Newtonian) counterparts. A distinctive feature of such hyperbolic systems is that their wave structure has finite propagation speeds given by the eigenvalues of the Jacobian matrices of the systems. Therefore, characteristic curves may cross during an evolution even for initially smooth initial data, and discontinuities may in turn develop along the course of such evolutions. As a consequence, standard finite difference schemes may show important deficiencies when dealing with nonlinear hyperbolic systems. Typically, first order accurate schemes are much too dissipative across discontinuities, while second order (or higher order) schemes produce spurious oscillations near discontinuities. High-resolution methods are all based on modified high-order finite-difference methods with the appropriate amount of numerical dissipation in the vicinity of a discontinuity to smooth out unphysical oscillations.

Finite difference (and finite volume) schemes [5, 6] provide numerical solutions of the discretised version of the partial differential equations (PDEs). Therefore, convergence properties under grid refinement must be enforced on such schemes to guarantee the validity of the numerical result (see [51] and references therein). As stated by the Lax-Wendroff theorem for hyperbolic systems of conservation laws, schemes written in *conservation form* converge to one of the so-called *weak solutions* of the PDEs (i.e. C^1 solutions in smooth parts of the flow and with a finite number of discontinuities). However, since there is no uniqueness for the initial value problem, the numerical scheme must guarantee convergence to the *physically admissible solution* among all weak solutions, a property whose mathematical characterisation was given by Lax for hyperbolic systems of conservation laws.

A conservative scheme for the hyperbolic system (10) can be easily formulated by using the corresponding integral form of the system of equations:

$$\int_\Omega \frac{1}{\sqrt{-g}} \frac{\partial \sqrt{\gamma}\mathbf{U}}{\partial x^0} d\Omega + \int_\Omega \frac{1}{\sqrt{-g}} \frac{\partial \sqrt{-g}\mathbf{F}^i}{\partial x^i} d\Omega = \int_\Omega \mathbf{S} d\Omega, \tag{57}$$

where Ω is a region of the 4-dimensional manifold enclosed within a 3-dimensional surface $\partial\Omega$ which is bounded by two spacelike surfaces $\Sigma_{x^0}, \Sigma_{x^0+\Delta x^0}$ and two timelike surfaces $\Sigma_{x^i}, \Sigma_{x^i+\Delta x^i}$. For numerical purposes the above relation can be written as:

$$\begin{aligned} \bar{\mathbf{U}}_{x^0+\Delta x^0} - \bar{\mathbf{U}}_{x^0} = & -\left(\int_{\Sigma_{x^1+\Delta x^1}} \sqrt{-g}\hat{\mathbf{F}}^1 dx^0 dx^2 dx^3 - \int_{\Sigma_{x^1}} \sqrt{-g}\hat{\mathbf{F}}^1 dx^0 dx^2 dx^3 \right) \\ & -\left(\int_{\Sigma_{x^2+\Delta x^2}} \sqrt{-g}\hat{\mathbf{F}}^2 dx^0 dx^1 dx^3 - \int_{\Sigma_{x^2}} \sqrt{-g}\hat{\mathbf{F}}^2 dx^0 dx^1 dx^3 \right) \end{aligned}$$

$$- \left(\int_{\Sigma_{x^3+\Delta x^3}} \sqrt{-g}\hat{\mathbf{F}}^3 dx^0 dx^1 dx^2 - \int_{\Sigma_{x^3}} \sqrt{-g}\hat{\mathbf{F}}^3 dx^0 dx^1 dx^2 \right) + \int_\Omega \mathbf{S} d\Omega, \tag{58}$$

where

$$\bar{\mathbf{U}} = \frac{1}{\Delta V} \int_{x^1}^{x^1+\Delta x^1} \int_{x^2}^{x^2+\Delta x^2} \int_{x^3}^{x^3+\Delta x^3} \sqrt{\gamma}\mathbf{U} dx^1 dx^2 dx^3 \,, \tag{59}$$

and

$$\Delta V = \int_{x^1}^{x^1+\Delta x^1} \int_{x^2}^{x^2+\Delta x^2} \int_{x^3}^{x^3+\Delta x^3} \sqrt{\gamma} dx^1 dx^2 dx^3. \tag{60}$$

The main advantage of this procedure is that those variables which obey a conservation law are conserved during the evolution, as long as the balance between the fluxes at the boundaries of the computational domain and the source terms is zero. The *numerical fluxes* appearing in Eq. (58), indicated by a hat symbol not to be confused with the same symbol indicating flat spacetime operators, are calculated at cell interfaces where the flow conditions can be discontinuous. Those numerical fluxes are approximations to the time-averaged fluxes across an interface, i.e.

$$\hat{\mathbf{F}}_{i+\frac{1}{2}} = \frac{1}{\Delta x^0} \int_{(x^0)^n}^{(x^0)^{n+1}} \mathbf{F}(\mathbf{U}(x_{i+\frac{1}{2}}, x^0))\, dx^0, \tag{61}$$

where the flux integral depends on the solution at the numerical interfaces, $\mathbf{U}(x_{i+1/2}, t)$, during the time step.

Godunov first proposed to calculate $\mathbf{U}(x_{i+1/2}, x^0)$ by exactly solving Riemann problems (initial value problems with discontinuous data) at every cell interface to obtain $\mathbf{U}(x_{i+1/2}, x^0) = \mathbf{U}(0; \mathbf{U}_i^n, \mathbf{U}_{i+1}^n)$, which denotes the Riemann solution for the (left and right) states $\mathbf{U}_i^n$, $\mathbf{U}_{i+1}^n$ along the ray $x/x^0 = 0$. This was a procedure of far-reaching consequences, as it was incorporated in the design of numerical schemes for solving Euler's equations of classical gas dynamics in the presence of shock waves, which led to major advances in the field. The derivation of the exact solution of the Riemann problem involves the computation of the full wave speeds to find where they lie in state space. This is a computationally expensive procedure, particularly for complex EOS and in multidimensions. Furthermore, for relativistic multidimensional flows, the coupling of all velocity components through the Lorentz factor results in the increase in the number of algebraic Rankine-Hugoniot conditions to consider in the case of shock waves and in solving a system of ODEs for the so-called rarefaction waves. In spite of this, the exact solution of the Riemann problem in *special* relativistic hydrodynamics has been derived [52, 53] (see also [3] for downloading a numerical code which implements the exact solution). Nevertheless, the computational inefficiency involved in the use of the exact solver in long-term numerical simulations motivated the gradual development of *approximate Riemann solvers*. These, being computationally much cheaper than the exact solver yield equally accurate results. They are based in the exact solution of Riemann problems corresponding to a new system of equations obtained by a suitable linearization of the original one. The spectral decomposition of the Jacobian matrices is on the basis of all such solvers, which extended ideas used for linear hyperbolic systems. This is the approach followed by an important subset of shock-capturing schemes, the so-called Godunov-type methods [54, 55].

The spatial accuracy of the numerical solution can be increased by reconstructing the primitive variables at the cell interfaces before the actual computation of the numerical fluxes. Diverse cell-reconstruction procedures are available in the literature (see references in [5, 6]) and have all been straightforwardly applied in relativistic hydrodynamics. Correspondingly, the temporal accuracy of the scheme can be improved by advancing in time the equations in integral form using the method of lines in tandem with a high-order, conservative Runge-Kutta method (see e.g. [3, 4]).

The main approaches extended from computational fluid dynamics to build HRSC schemes in relativistic hydrodynamics can be divided in the following broad categories (see [3] for further details on such classification):

(i) HRSC schemes based on **Riemann solvers** (upwind methods): Developments include both, solvers relying on the exact solution of the Riemann problem: [52, 53], relativistic PPM [56], Glimm's random choice method [57], and two-shock approximation [58, 59], as well as **linearized solvers** based on local linearizations of the Jacobian matrices of the flux-vector Jacobians, e.g. Roe-type Riemann solvers (Roe-Eulderink: [10]; Local Characteristic Approach: [13, 60, 9]), primitive-variable formulation: [61], and Marquina Flux Formula: [62].

(ii) HRSC schemes sidestepping the use of characteristic information (**symmetric schemes** with nonlinear numerical dissipation): Various approaches have been undertaken recently, including those by [63] (Lax-Wendroff scheme with conservative TVD dissipation terms), [64] (Lax-Friedrichs or HLL schemes with third-order ENO reconstruction algorithms), [65] (non-oscillatory central differencing), and [66, 67] (semidiscrete central scheme of Kurganov-Tadmor [68]).

Other approaches worth mentioning include:

(i) Schemes based on **artificial viscosity**, both for nonconservative and conservative formulations of the GRHD equations [14, 65].

(ii) **Flux-corrected transport** scheme [69], a flux-limiter scheme where the numerical flux is obtained from a high-order flux (e.g. Lax-Wendroff) in the smooth regions and from a low order flux (e.g. the flux from some monotone method) near discontinuities.

(iii) **Smoothed particle hydrodynamics** [70, 71] for many body systems. In these two references the relativistic hydrodynamics equations are formulated in conservation form, a feature from which [71] profited to devise a consistent artificial viscosity treatment. Furthermore, in [70] dissipation terms were constructed in analogy to terms in Riemann-solver-based methods.

As mentioned above the interested reader is addressed to the review article by [3] for a complete list of references on this topic as well as for an in-depth comparison of the performance of the various numerical approaches avilable.

Concerning the GRMHD equations the numerical advantage of using Eq. (58) for the conserved variables is not entirely apparent for the magnetic field components, as there is no guarantee that such a procedure conserves the divergence of the magnetic field during a numerical evolution. The main physical implication of the divergence constraint is that the magnetic flux through a closed surface $\hat{A}$ enclosing a volume $\hat{V}$ is zero. This flux can be calculated as a surface integral of the "densitized" magnetic field

(i.e. $B^{\dagger i} \equiv \sqrt{\bar{\gamma}} B^i$, with $\bar{\gamma} = \gamma/\hat{\gamma}$, $\hat{\gamma}$ denoting the flat spacetime metric determinant) as

$$\Phi_{\rm T} = \oint_{\hat{A}=\partial\hat{V}} \mathbf{B}^\dagger \cdot d\hat{\mathbf{A}} = \int_{\hat{V}} \hat{\nabla} \cdot \mathbf{B}^\dagger d\hat{V} = 0, \tag{62}$$

after applying Gauss theorem and the magnetic field divergence-free constraint. This equation implies that no source of magnetic flux exists inside the volume $\hat{V}$ and, therefore, the magnetic flux is a conserved quantity as $\frac{\partial \Phi_{\rm T}}{\partial t} = 0$.

In addition, if one considers a generic surface $\hat{A}$ (without the restriction of having to enclose a volume), the time variation of the magnetic flux through this surface is

$$\frac{\partial \Phi}{\partial t} = \frac{\partial}{\partial t} \int_{\hat{A}} \mathbf{B}^\dagger \cdot d\hat{\mathbf{A}} = \int_{\hat{A}} \left[\hat{\nabla} \times \left(\mathbf{v}^\dagger \times \mathbf{B}^\dagger \right) \right] \cdot d\hat{\mathbf{A}} = - \oint_{\hat{C}=\partial\hat{A}} \mathbf{E}^\dagger \cdot d\hat{\mathbf{l}}, \tag{63}$$

where we have used the induction equation (19) and Stokes theorem to transform the surface integral into a line integral along the curve $\hat{C}$ enclosing $\hat{A}$, and the equality $\mathbf{E}^\dagger = \mathbf{v}^\dagger \times \mathbf{B}^\dagger$. The previous two properties allow to design a numerical algorithm to solve the induction equation and the divergence constraint in a way that ensures the conservation of the magnetic flux. A common choice among the methods for doing so is the so-called constrained transport method [72, 73], and its *flux*-constrained transport extension [30]. The interested reader is addressed to [23, 74] for further details.

The current approaches to solve the RMHD equations within HRSC schemes also fall within the categories mentioned above, yet the degree of development achieved thus far is somewhat more limited here than in the purely hydrodynamical case. Methods based on Riemann solvers have been initiated in special relativity by [28], who provided eigenvector sets for degenerate states, [30], whose most distinct feature is that the cell reconstruction is not done on primitive variables, [75], which provide right- and left-eigenvectors in covariant variables, but restricted to the one-dimensional case, and [23, 31], who derived a complete set of right- and left-eigenvectors in conserved variables, valid even for degenerate states, as well as in general relativity by [76, 23]. On the other hand symmetric schemes (namely, the HLL scheme and the method devised by Kurganov-Tadmor [68]) are being currently employed by a growing number of groups in GRMHD [63, 19, 21, 22, 23]. It is worth to emphasize that all references listed here use conservative formulations of the GRMHD equations. Artificial viscosity approaches are advocated by [77, 17].

To close this section we note that a distinctive feature of the numerical solution of the GRHD/GRMHD equations - not existing in the Newtonian case - is that while the numerical algorithm updates the vector of conserved quantities, the numerical code makes extensive use of the primitive variables throughout. Those appear repeatedly in the solution procedure, e.g. in the characteristic fields, in the solution of the Riemann problem, and in the computation of the numerical fluxes.

For spacelike foliations of the spacetime (3+1) the relation between the two sets of variables is implicit. Hence, iterative (root-finding) algorithms are required. Those have been developed for all existing formulations [10, 9, 11]. For practical purposes this procedure may lead to accuracy losses in regions of low density and small velocities, apart from being computationally inefficient. We note, however, that for null foliations of the spacetime, the procedure of connecting primitive and conserved variables is explicit for the GRHD case for a perfect fluid EOS, a direct consequence of the particular form of the Bondi-Sachs metric (see [11]). Finally, the recovery of primitive variables in the GRMHD case is quite more involved than in the GRHD case, due to the augmented complexity of the equations for the former system. Diverse procedures are reported in [28, 23, 78]

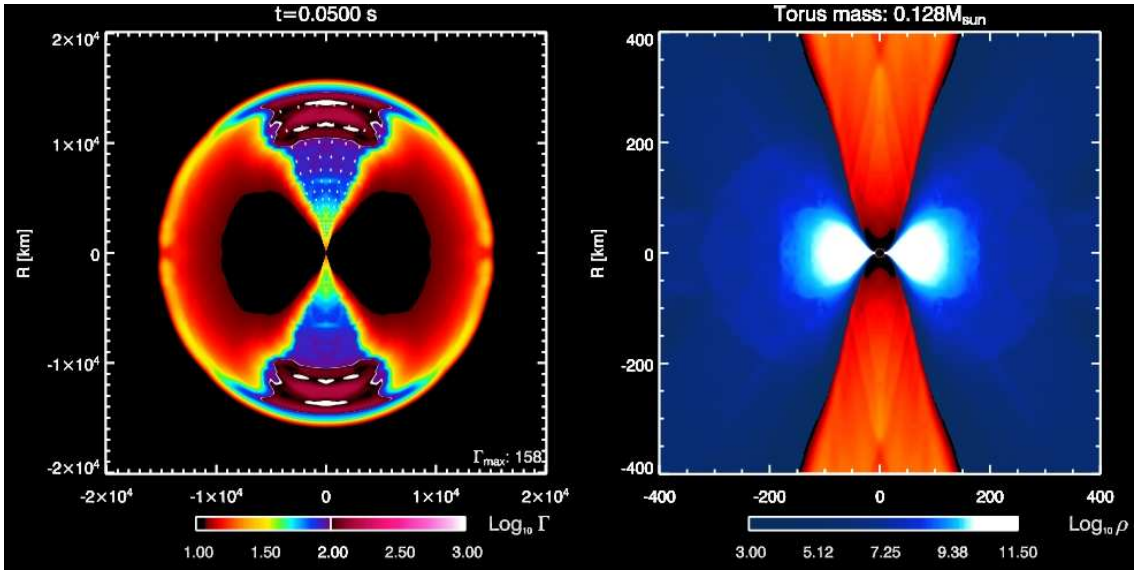

Figure 1. Ultrarelativistic outflow from the remnant of the merger of a binary neutron star system. The figure shows the gamma-ray burst model B01 from [79] corresponding to a time $t = 50$ ms after the start of the energy deposition, at a rate of 2×10^{51} erg/s. The (r, θ) grid resolution in this axisymmetric simulation is 1000×200. The outflow in the white-coloured regions in the left panel (closer to the black hole), magnified in the right panel, achieves Lorentz factors of ~ 100, with terminal values of about 1000. See [79] for further details.

6. Some examples in numerical astrophysics

Both, hydrodynamical and MHD numerical simulations are nowadays an essential tool in theoretical astrophysics, to model either classical or relativistic sources. These simulations strongly rely on the accuracy of the underlying numerical codes, which is calibrated through stringent convergence tests (see [51]) and, when possible, through comparisons of the numerical solutions with analytic results. Typical testbeds to assess numerical codes include shock tube tests (Riemann problems), shock reflection tests, or stationary, spherically-symmetric perfect fluid accretion on to both Schwarzschild and Kerr black holes.

In recent years, the morphology and dynamics of most scenarios present in the arena of relativistic astrophysics have been already investigated to varying degrees of sophistication. The examples are numerous, much too abundant to be covered here with a minimum detail: Heavy ion collisions, dynamics and stability of relativistic jets both at pc and Kpc scales (the latter two situations are amenable to investigations in the special relativistic limit), gamma-ray burst models, gravitational collapse to neutron stars and black holes, accretion on to black holes, jet formation, pulsations and instabilities of rotating relativistic stars, and binary neutron star mergers. In the remaining of the paper we give a glimpse of the state-of-the-art achieved in the modelling of some of these scenarios, providing pointers for further reading.

Relativistic outflows from mergers of compact objects. Relativistic thick discs (or tori) orbiting around black holes may form after the gravitational collapse of the core of a rotating massive star ($M > 25 M_\odot$) or after a neutron star binary merger. Such accreting torus plus black hole system is the most likely candidate to be

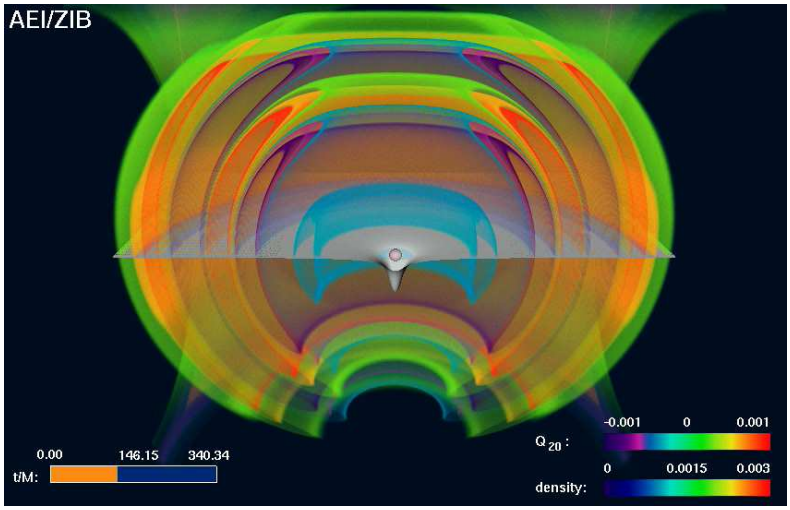

Figure 2. Gravitational radiation from the collapse of a neutron star to a rotating black hole [49]. The figure shows a snapshot in the evolution of the system once the black hole has been formed and the gravitational waves are being emitted in large amounts. See [49] for further details.

the mechanism powering gamma-ray bursts. Part of the large amounts of the energy released by accretion is deposited in the low-density region along the rotation axis, where the heated gas expands in a jet-like fireball.

Figure 1 shows a snapshot at time $t = 0.05$ s of a GRHD axisymmetric simulation of the launch and evolution of a relativistic outflow driven by energy deposition by neutrino-antineutrino annihilation in the vicinity of a black hole plus accretion torus system (model B1 of [79]). The left panel displays the logarithm of the Lorentz factor in the entire computational domain, while the right panel focuses on the innermost regions closer to the central black hole, depicting the logarithm of the rest-mass density. Since in this simulation the system is the remnant of a binary neutron star merger, it naturally provides a baryon-free channel along the rotation axis through which the outflow can reach ultrarelativistic velocities. Indeed, terminal Lorentz factors of about 1000 are attained for initial energy deposition rates of some 10^{48} erg/s per stereoradian. As shown in Fig. 1 the outflow is strongly collimated due to the presence of the accretion torus, which, in turn, makes the gamma-ray emission very weak outside of the polar cones. The calculations reported by [79] predict that about one out of a hundred neutron star mergers produces a detectable gamma-ray burst, as its ultrarelativistic jet happens to be sent along the line of sight‡.

Gravitational collapse and black hole formation. Most numerical investigations in general relativistic rotational collapse have been (and still are) concerned with the question of black hole formation. One of the milestones in the field of Numerical Relativity were the axisymmetric simulations by Stark and Piran [80], who studied the collapse of rotating relativistic polytropes to black holes and first computed the associated gravitational radiation.

This problem has been revisited in recent years by a number of groups, employing more suitable formulations of Einstein's equations such as BSSN and more advanced

‡ The interested reader is addressed to `www.mpa-garching.mpg.de/mpa/research/current_research/hl2004-9/hl2004-9-en.html` for animations of representative simulations of such relativistic outflows.

numerical methodology [81, 82, 83, 48, 84, 49]. In particular, in [48] the gravitational collapse of uniformly rotating neutron stars to Kerr black holes was studied in three dimensions using the `cactus/whisky` code for Numerical Relativity. Long-term simulations were possible by excising the region of the computational domain which includes the curvature singularity when the black hole forms and lies within the apparent horizon. It was found that for sufficiently high angular velocities, the collapse can lead to the formation of a differentially rotating unstable disk. Gravitational waveforms from such simulations were reported in [84]. Despite good qualitative agreement was found with the waveforms reported in previous axisymmetric simulations [80], the new-computed amplitudes were about an order of magnitude smaller due to the more realistic rotation rates of the collapse progenitors.

Very recently, [49] have suceeded in computing the gravitational waveforms from the gravitational collapse of a neutron star to a rotating black hole well beyond what had so far been possible, even providing information on the ringdown signal through which the formed black hole relaxes to its asymptotic, stationary state. These new three-dimensional computations, contrary to most approaches, did not excise the region inside the apparent horizon once the black hole forms, so as to remove the curvature singularity and improve, in principle, the numerical stability. Instead, they were performed without excision, which, combined with suitable singularity-avoiding gauge conditions and the use of minute (artificial) Kreiss-Oliger type numerical dissipation in the spacetime evolution and gauge equations, improved dramatically their long-term stability. An example of this remarkable result is provided by Fig. 2 which shows a snapshot during the evolution of one of the collapse models of [49]§. The figure displays the gravitational waveform train extracted by matching the numerical spacetime with non-spherical perturbations of a Schwarzschild black hole described in terms of gauge-invariant odd- and even-parity metric perturbations, namely the lowest order odd-parity multipole Q_{20}. Also in the central parts of the figure is visible the collapse of the lapse function and the formation of a rotating black hole. The study of [49] shows that (stellar mass) black hole formation events would produce gravitational radiation potentially detectable by the present detectors (LIGO/Virgo) in the case the events took place at Galactic distances.

Magneto-rotational stellar core collapse. Stars with initial masses larger than $\sim 9M_\odot$ end their thermonuclear evolution developing a core composed of iron group nuclei, which is dynamically unstable against gravitational collapse. The core collapses to a neutron star releasing gravitational binding energy of the order $\sim 3\times10^{53}$ erg $(M/M_\odot)^2(R/10\text{ km})^{-1}$, sufficient to power a (Type II/Ib/Ic) supernova explosion. The current knowledge of the underlying physics in supernova explosions has gradually accumulated through advanced simulations in (post-)Newtonian gravity and hydrodynamics. These show how sensible the explosion mechanism is to the details of the post-bounce evolution: gravity, the nuclear EOS and the properties of the nascent neutron star, the treatment of the neutrino transport, and the neutrino-matter interaction.

The first axisymmetric simulations of rotational core collapse to neutron stars which incorporated a relativistic treatment of gravity were performed by [85, 39, 86, 37, 45]. These simulations employed simplified models to account for the thermodynamics of the process, in the form of a polytropic EOS conveniently modified to account for

§ Animations of this evolution are available at `http://numrel.aei.mpg.de`

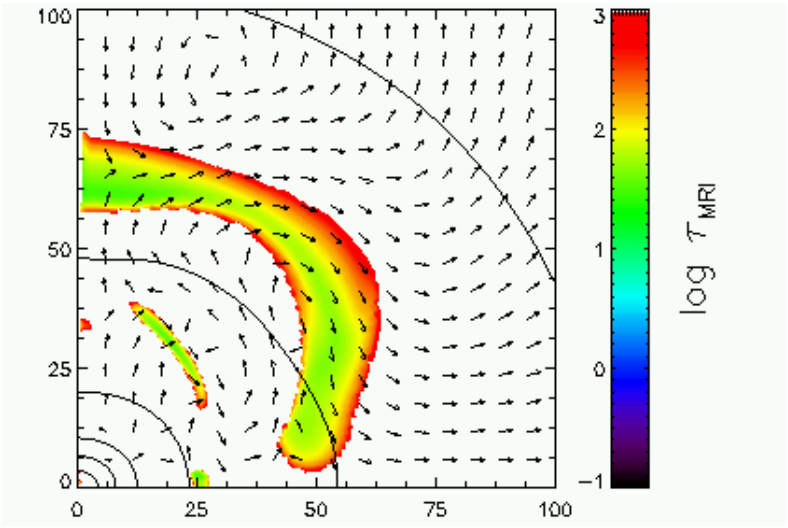

Figure 3. Magneto-rotational instability in magneto-rotational collapse at the end of one of the simulations performed by [74, 93]. Color coded is the logarithm of the timescale of the fastest growing unstable mode of the magneto-rotational instability, in ms. Arrows indicate the velocity field and the isocontours the rest-mass density. The axes are in km.

the stiffening of the matter once nuclear matter density is reached. The inclusion of relativistic effects results primarily in the possibility to achieve deeper effective potentials. Moreover, higher densities than in Newtonian models are reached during bounce, and the resulting proto-neutron star is more compact. On the other hand, relativistic simulations of microphysically detailed core collapse beyond spherical symmetry are just beginning to be available [87, 88]. These simulations employ both the CFC and BSSN formulations of Einstein's equations, and have been carried out using state-of-the-art numerical codes, both in spherical polar coordinates (the `CoCoNut` code of [40]) and in Cartesian coordinates (the `cactus/carpet/whisky` codes; see [89, 90, 48, 87] and references therein). The simulations reported by [87, 88] allow for a direct comparison with models with simple (polytropic) EOS and same rotation parameters as those of [86, 45, 37]. This sheds light on the influence of rotation and of the EOS on the gravitational waveforms. This comparison shows that for microphysical EOS the influence of rotation on the collapse dynamics and waveforms is somewhat less pronounced than in the case of simple EOS. In particular, the most important result of these investigations is the supression of core collapse with multiple centrifugal bounces and its associated Type II gravitational waveforms. As a result, the improved simulations of [88, 87] reveal an enhanced uniformity on the gravitational wave signal from core bounce.

On the other hand, neutron stars have intense magnetic fields ($\sim 10^{12} - 10^{13}$ G), which renders mandatory their inclusion in core collapse simulations. In recent years, an increasing number of authors have performed axisymmetric magneto-rotational simulations (within the so-called ideal MHD limit) employing Newtonian treatments of the magneto-hydrodynamics, the gravity, and of the microphysics (see [91] and references therein). The weakest point of all existing simulations to date is the fact that the strength and distribution of the initial magnetic field in the core are essentially unknown. The available simulations show that for realistic weak initial fields, $\leq 10^{11}$ G, there are no major differences in the collapse dynamics nor in

the resulting gravitational wave signal, when comparing with purely hydrodynamical simulations. However, strong initial fields ($\geq 10^{11}$ G) manage to slow down the core efficiently, leading even to retrograde rotation in the proto-neutron star, which causes qualitatively different dynamics and gravitational wave signals.

Very recently, the first magneto-rotational core collapse axisymmetric simulations in full general relativity have been reported [92, 74, 93], based upon both, the BSSN and CFC formulations of Einstein's equations and for polytropic and microphysical EOS with deleptonization and neutrino pressure. In particular, the most recent results by [93] show that for the case of core collapse models with microphysics and realistic values for the magnetic fields of the collapse progenitors, the saturation of the magnetic field cannot be reached within dynamical time scales by winding up the poloidal magnetic field into a toroidal one, at least in axisymmetry. Comparing with models with simplified EOS, microphysical collapse models are found to lead to a more complex structure of the poloidal magnetic field due to convective motions surrounding the inner region of the proto-neutron star, and exhibit a wind-up of the magnetic field (through the Ω-dynamo mechanism) that is more efficient than for simplified models for comparable rotation rates, an effect due to the larger compression of the poloidal component during the collapse.

Figure 3 shows a snapshot of a magneto-rotational collapse simulation at the end of the evolution, for a particular model of the sample analyzed by [74, 93]. Depicted in white in this figure are the regions where the condition for the ocurrence of the so-called magneto-rotational instability (MRI hereafter; see [94] and references therein for details) is not fulfilled or the timescale of the fastest growing mode exceeds 1 s. It is found that a significant fraction of the newly-formed proto-neutron star, as well as the region behind the shock at the moment of its formation, are affected by the MRI. We note that the presence of convectively unstable regions in microphysical collapse models enhances the appearance of the instability just outside the inner region of the proto-neutron star as compared to simplified models. In principle, thus, MRI could cause the exponential growth of the magnetic field on dynamical timescales, reaching saturation in those regions, becoming important for the dynamics. However, it is worth stressing that the value of the magnetic field at which saturation appears is still unknown. This is, indeed, the key issue in order to establish the actual effects of the MRI on the collapse dynamics and on the gravitational waveforms emitted in the process, an issue which future GRMHD simulations have to address.

Binary neutron star coalescence. Many current efforts in numerical relativistic astrophysics aim at simulating binary neutron star coalescence. Neutron star binaries are among the most promising sources of high-frequency gravitational radiation to be detected by the various ground-based interferometers worldwide and, in addition, such mergers are behind the accepted mechanism to explain short-duration GRBs. The gravitational waveform during the plunge and merge of two compact stars cannot be computed using post-Newtonian methods but requires the whole machinery of GRHD/GRMHD and Numerical Relativity. Its accurate simulation is a major challenge as the scenario involves strong gravitational fields, ultrarelativistic flows, and the formation of curvature singularities. The most advanced simulations in full general relativity are those performed by Shibata and coworkers (see [50] and references therein). Their numerical code allows to carry out long-term simulations for both irrotational and corotational binaries of equal or unequal masses, from the innermost stable circular orbit up to the formation and ringdown of the final collapsed object

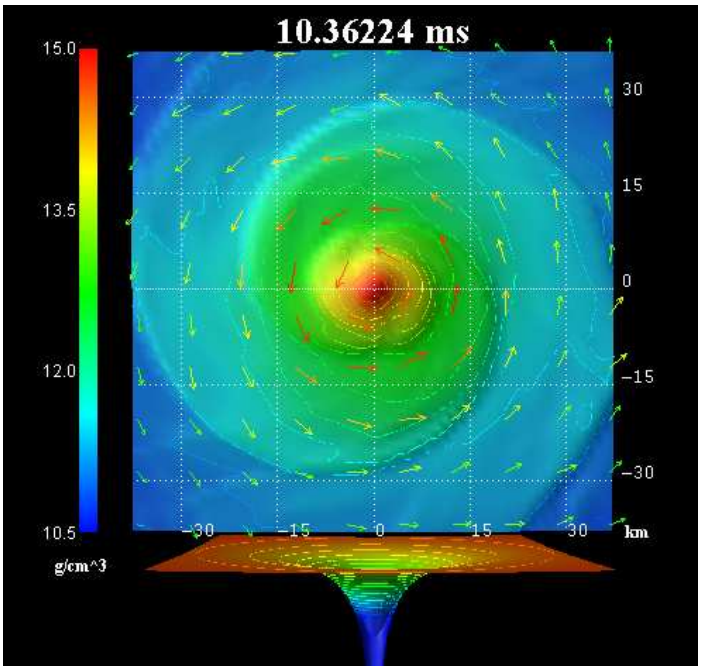

Figure 4. Isodensity contours in the equatorial plane for the merger of a $1.35M_\odot$-$1.35M_\odot$ neutron star binary. Vectors indicate the local velocity field (v^x, v^y). The image corresponds to the final snapshot of the evolution, $t = 10.36$ ms. The outcome of the merger is the delayed formation of a black hole, as signalled by the collapse of the lapse function shown in the lower panel of the image. Simulation performed by [50].

(either a black hole or a stable neutron star), and for perfect fluid EOS or realistic (nuclear) EOS. The code also includes apparent horizon finders and can extract the gravitational waveforms emitted in the collisions. The parameter-space survey carried out by Shibata *et al.* [50] has shown how sensitive the final outcome of the merger is to the initial compactness of the neutron stars before the plunge.

A representative example of the dynamics of an equal mass ($1.35M_\odot$-$1.35M_\odot$) binary neutron star merger is shown in Fig. 4 (see [50] for further details). The main panel of this figure displays a snapshot of the velocity field and rest-mass isodensity contours in the equatorial plane at the final time of the evolution, $t = 10.36$ ms. The lower panel shows the topology of the lapse function at the same final time of the evolution. The end product of this particular merger is the delayed formation of a rotating black hole‖.

7. Summary

Formulations of the equations of (inviscid) general relativistic hydrodynamics and (ideal) magneto-hydrodynamics have been discussed, along with methods for their numerical solution. We have shown that both systems can be cast as first-order, hyperbolic systems of conservation laws, following the explicit choice of an Eulerian observer and suitable fluid and magnetic field variables, which allows to design numerical strategies especific to such hyperbolic systems. During the last fifteen years, the so-called (upwind) high-resolution shock-capturing schemes based on Riemann

‖ Animations of such simulations are available at `www.esa.c.u-tokyo.ac.jp/shibata/index.html`

solvers have been successfully extended from classical to relativistic fluid dynamics, both special and general. The article has also presented a brief overview of such numerical techniques for hyperbolic systems of conservation laws, providing a handful of state-of-the-art examples of their applicability to general relativistic fluids and magneto-fluids in characteristic scenarios of relativistic astrophysics.

Nowadays, general relativistic hydrodynamical simulations in relativistic astrophysics are routinely performed by a growing number of groups. This is particularly true within the test-fluid approximation but also for dynamical spacetimes. Indeed, for the latter case, it is worth mentioning the long-term, numerically stable formulations of Einstein's equations (or accurate enough approximations) that have been proposed by several Numerical Relativity groups worldwide in recent years. Some of these have also been briefly discussed here. The paradigm which the numerical relativist is currently confronted with has suddenly changed for the best. Accurate and long-term stable, *coupled* evolutions of the GRHD/GRMHD equations and Einstein's equations are just becoming possible in three-dimensions (benefited from the steady increase in computing power), allowing for the study of interesting relativistic astrophysics scenarios for the first time, such as gravitational collapse, accretion onto black holes, and binary neutron star mergers. While major recent advances have also been achieved for the MHD equations, the astrophysical applications investigated so far are still limited. However, there can be little doubts that this field is bound to witness significant developments in the near future.

Acknowledgments

This research has been supported by the Spanish *Ministerio de Educación y Ciencia* (grant AYA2004-08067-C03-01). I am very grateful to Miguel Angel Aloy, Luca Baiotti, Luciano Rezzolla, and Masaru Shibata for providing some of the illustrative, colourful figures of this paper. It is a great pleasure to acknowledge the organizers of the VII Mexican School on Gravitation and Mathematical Physics for their invitation to deliver these lectures and for setting up such a nice school.

References

[1] Anile, M.M., *Relativistic fluids and magneto-fluids*, Cambridge University Press (1989)
[2] Ibáñez et al, in Proc. Workshop *Godunov Methods: Theory and Applications*, Ed. E.F. Toro, Kluwer Academic/Plenum Publishers, New York (2001)
[3] Martí, J.M. and Müller, E., Liv. Rev. Relativ., **6**, 7 (2003)
[4] Font, J.A., Liv. Rev. Relativ., **6**, 4 (2003)
[5] LeVeque, R.J., *Numerical methods for conservation laws*, Birkhäuser, Basel (1992)
[6] Toro, E.F., *Riemann solvers and numerical methods for fluid dynamics*, Springer Verlag, Berlin (1997)
[7] Chorin and Marsden, *A mathematical introduction to fluid mechanics*, Springer (1984)
[8] Wilson, J. R., Astrophys. J., **173**, 431 (1972)
[9] Banyuls, F., Font, J.A., Ibáñez, J.M., Martí, J.M. and Miralles, J.A., Astrophys. J., **476** 221 (1997)
[10] Eulderink, F. and Mellema, G., Astron. Astrophys., **284**, 652 (1994).
[11] Papadopoulos, P. and Font, J. A., Phys. Rev. D **61** 024015 (2000).
[12] York, J., in *Sources of Gravitational Radiation*, edited by L. Smarr (Cambridge University Press, Cambridge, England, 1979).
[13] Martí, J.M., Ibáñez, J.M., and Miralles, J.A., Phys. Rev. D, **43**, 3794 (1991)
[14] Norman, M. L. and Winkler, K-H., in Astrophysical Radiation Hydrodynamics, Reidel Publishing Company, 449-475 (1986)

[15] Font, J. A., Miller, M., Suen, W. M. and Tobias, M., Phys. Rev. D, **61**, 044011 (2000)
[16] Koide, S., Shibata, K., and Kudoh, T., Astrophys. J., **495**, L63 (1998)
[17] De Villiers, J. and Hawley, J. F., Astrophys. J., **589**, 458 (2003)
[18] Baumgarte, T. W. and Shapiro, S. L., Astrophys. J., **585**, 921 (2003)
[19] Gammie, C. F., McKinney, J. C., and Tóth, G., Astrophys. J., **589**, 444 (2003)
[20] Komissarov, S. S., MNRAS, **359**, 801 (2005)
[21] Duez, M. D., Liu, Y. T., Shapiro, S. L., & Stephens, B. C., Phys. Rev. D, **72**, 024028 (2005)
[22] Shibata, M. & Sekiguchi, Y., Phys. Rev. D, **72**, 044014 (2005)
[23] Antón, L., Zanotti, O., Miralles, J.A., Martí, J.M., Ibáñez, J.M., Font, J.A. and Pons, J.A., Astrophys. J., **637**, 296 (2006)
[24] Neilsen, D., Hirschmann, E. W., and Millward, R. S., Class. Quantum Grav. **23**, S505 (2006)
[25] Mizuno, Y., Nishikawa, K., Koide, S., Hardee, P., and Fishman, G. J., 2006, astro-ph/0609004
[26] Anile, A. M. and Pennisi, S., Annales de l'Institut Henri Poincaré, **46**, 27 (1987)
[27] van Putten, M. H. P. M., Comm. Math. Phys., **141**, 63 (1991)
[28] Komissarov, S. S., MNRAS, **303**, 343 (1999)
[29] Koldoba, A. V., Kuznetsov, O. A., & Ustyugova, G. V., MNRAS, **333**, 932 (2002)
[30] Balsara, D., Astrophys. J. Supp., **132**, 83 (2001)
[31] Antón L., 2007, PhD Thesis, University of Valencia.
[32] Brio, M. and Wu, C. C., J. Comput. Phys., **75**, 400 (1988)
[33] Campanelli, M., these proceedings.
[34] Alcubierre, M., AIP Conference Proceedings, **758**, 193-207 (2005)
[35] Isenberg, J.A., "Waveless approximation theories of gravities", University of Maryland Preprint (1978, unpublished), gr-qc/0702113.
[36] Wilson, J.R., Mathews, G.J., and Marronetti, P., Phys. Rev. D **54**, 1317 (1996)
[37] Shibata, M. and Sekiguchi, Y., Phys. Rev. D, **69** 084024 (2004)
[38] Cook, G. B., Shapiro, S. L. and Teukolsky, S. A., 1996, Phys. Rev. D, **53**, 5533
[39] Dimmelmeier, H., Font, J.A. and Müller, E., Astron. Astrophys., **388**, 917 (2002)
[40] Dimmelmeier, H., Novak, J., Font, J.A., Ibáñez, J.M., and Müller, E., Phys. Rev. D, **71**, 064023 (2005)
[41] Saijo, M., Phys. Rev. D, **71**, 104038 (2005)
[42] Dimmelmeier, H., Stergioulas, N., and Font, J.A., MNRAS, **368**, 1609 (2006)
[43] Oechslin, R., Rosswog, S., and Thielemann, F.-K., Phys. Rev. D, **65**, 103005 (2002)
[44] Faber, J. A., Grandclément, P., and Rasio, F. A., Phys. Rev. D, **69**, 124036 (2004)
[45] Cerdá-Durán, P., Faye, G., Dimmelmeier, H., Font, J. A., Ibáñez, J. M., Müller, E. and Schäfer, G., Astron. Astrophys., **439** 1033-1055 (2005)
[46] Shibata, M. and Nakamura, T., Phys. Rev. D, **52**, 5428 (1995)
[47] Baumgarte, T.W. and Shapiro, S.L., Phys. Rev. D, **59**, 024007 (1999)
[48] Baiotti, L., Hawke, I., Montero, P.J., Loeffler, F., Rezzolla, L., Stergioulas, N., Font, J.A., and Seidel, E., Phys. Rev. D, **71**, 024035 (2005)
[49] Baiotti, L. and Rezzolla, L., Phys. Rev. Lett., **97**, 141101 (2006)
[50] Shibata, M., Taniguchi, K., and Uryū, K., Phys. Rev. D, **71**, 084021 (2005)
[51] Choptuik, M., these proceedings.
[52] Martí, J.M. and Müller, E., J. Fluid Mech., **258** 317-333 (1994)
[53] Pons, J.A., Martí, J.M. and Müller, E., J. Fluid Mech., **422** 125-139 (2000)
[54] Harten, A. and Lax, P. D. and van Leer, B., SIAM Review, **25**, 35 (1983)
[55] Einfeldt, B., SIAM J. Num. Anal., **25**, 294 (1988)
[56] Martí, J.M. and Müller, E., J. Comput. Phys., **123** 1-14 (1996)
[57] Wen, L., Panaitescu, A., and Laguna, P., Astrophys. J., **486** 919-927 (1997)
[58] Balsara, D., J. Comput. Phys., **114** 284-297 (1994)
[59] Dai, W. and Woodward, P., SIAM J. Sci. Comput., **18** 957-981 (1997)
[60] Font, J.A., Ibáñez, J.M., Martí, J.M., and Marquina, A., Astron. Astrophys., **282** 304-314 (1994)
[61] Falle, S. A. E. G. and Komissarov, S. S., Mon. Not. R. Astron. Soc., **278** 586-602 (1996)
[62] Donat, R., Font, J. A., Ibáñez, J. M. and Marquina, A., J. Comput. Phys., **146** 58-81 (1998)
[63] Koide, S., Shibata, K. and Kudoh, T., Astrophys. J., **495** L63-L66 (1998)
[64] Del Zanna, L. and Bucciantini, N., Astron. Astrophys., **390** 1177-1186 (2002)
[65] Anninos, P. and Fragile, P. C., Astrophys. J. Suppl. Ser., **144** 243-257 (2002)
[66] Lucas-Serrano, A., Font, J. A., Ibáñez, J. M. and Martí, J. M., Astron. Astrophys., **428** 703-715 (2004)
[67] Shibata, M. and Font, J.A., Phys. Rev. D, **72** 047501 (2005)
[68] Kurganov, A. and Tadmor, E., J. Comput. Phys., **160** 214 (2000)

[69] Schneider, V., Katscher, V., Rischke, D. H., Waldhauser, B., Marhun, J. A. and Munz, C.-D., J- Comput. Phys., **105** 92-107 (1993)
[70] Chow, E. and Monaghan, J. J., J. Comput. Phys., **134** 296-305 (1997)
[71] Siegler, S. and Riffert, H., Astrophys. J., **531** 1053-1066 (2000)
[72] Evans, C. and Hawley, J. F., Astrophys. J., **332** 659-677 (1988)
[73] Tóth, G., J. Comput. Phys., **161** 605-652 (2000)
[74] Cerdá-Durán, P. and Font, J.A., Class. Quantum Grav., in press (2006), astro-ph/0703593
[75] Koldoba, A. V., Kuznetsov, O. A. and Ustyugova, G. V., MNRAS, **333** 932-942 (2002)
[76] Komissarov, S.S., MNRAS, **359** 801-808 (2005)
[77] Yokosawa, M., Publ. Astron. Soc. Japan, **45** 207-218 (1993)
[78] Noble, S.C., Gammie, C.F., McKinney, J.C., and Del Zanna, L., ApJ, **641** 626-637 (2006)
[79] Aloy, M. A., Janka, H.-T., and Müller, E., Astron. Astrophys., **436**, 273-311 (2005)
[80] Stark, R.F. and Piran, T., Phys. Rev. Lett., **55**, 891 (1985)
[81] Shibata, M., *Prog. Theor. Phys.* **104**, 325 (2000)
[82] Shibata, M. and Shapiro, S.L., Astrophys. J., **572**, L39 (2002)
[83] Duez, M.D., Liu, Y.T., Shapiro, S.L., and Stephens, B.C., Phys. Rev. D, **69**, 104030 (2004)
[84] Baiotti, L., Hawke, I., Rezzolla, L., and Schnetter, E., Phys. Rev. Lett., **94**, 131101 (2005)
[85] Dimmelmeier, H., Font, J.A. and Müller, E., ApJ, **560**, L163 (2001)
[86] Dimmelmeier, H., Font, J.A. and Müller, E., Astron. Astrophys., **393**, 523 (2002)
[87] Ott, C.D., Dimmelmeier, H., Marek, A., Janka, H.-T., Hawke, I., Zink, B., and Schnetter, E., astro-ph/0609819 (2006)
[88] Dimmelmeier, H. Ott, C.-D., Marek, A., Janka, H.-Th., and Müller, E., astro-ph/0702305 (2007)
[89] `http://www.cactuscode.org`
[90] Schnetter, E., Hawley, S.H., and Hawke, I., Class. Quantum Grav. **21**, 1465 (2004)
[91] Obergaulinger, M., Aloy, M.A., Dimmelmeier, H., and Müller, E., Astron. Astrophys., **457**, 209 (2006)
[92] Shibata, M., Phys. Rev. D **74** 104026 (2006)
[93] Cerdá-Durán, P., Font, J.A., and Dimmelmeier, H., Astron. Astrophys., submitted, eprint arXiv:astro-ph/0703597 (2007)
[94] Balbus, S. A., and Hawley, J. F., Astrophys. J., **376**, 214 (1991)